

RSC Advances



This is an *Accepted Manuscript*, which has been through the Royal Society of Chemistry peer review process and has been accepted for publication.

Accepted Manuscripts are published online shortly after acceptance, before technical editing, formatting and proof reading. Using this free service, authors can make their results available to the community, in citable form, before we publish the edited article. This *Accepted Manuscript* will be replaced by the edited, formatted and paginated article as soon as this is available.

You can find more information about *Accepted Manuscripts* in the [Information for Authors](#).

Please note that technical editing may introduce minor changes to the text and/or graphics, which may alter content. The journal's standard [Terms & Conditions](#) and the [Ethical guidelines](#) still apply. In no event shall the Royal Society of Chemistry be held responsible for any errors or omissions in this *Accepted Manuscript* or any consequences arising from the use of any information it contains.

Monodisperse CuS Nanodisks: Low-temperature Solvothermal Synthesis and Enhanced Photocatalytic Activity

Yu-Qiao Zhang, Bo-Ping Zhang, Li-Feng Zhu*

School of Materials Science and Engineering, University of Science and Technology Beijing,
Beijing 100083, China.

ABSTRACT: Controllable synthesis of uniformly disk-shaped CuS nanostructures with a narrow size distribution was realized by a low-temperature (150 °C) solvothermal process using polyvinyl pyrrolidone (PVP) as the surfactant. Monodispersed nanodisks of a pure CuS phase with an average diameter of ca. 500 nm could be obtained at a specific S/Cu molar ratio ($x_{S/Cu}$) of raw materials, which was revealed to affect the phase structure and morphology of the product but the influence of PVP content (x_{PVP}) is limited. The CuS nanodisks exert a broad absorption in the visible region and superior photocatalytic performances to the degradation of RhB whose decomposition rate reaches 93% in 2 h, indicating a potential application in the field of wastewater treatment.

KEYWORDS: CuS; Nanodisks; Photocatalysis; Solvothermal Method

* E-mail address: bpzhang@ustb.edu.cn Tel: +86-10-62334195 fax: +86-10-62334195.

Address: No.30 Xueyuan Road, Haidian Zone Beijing, Beijing 100083, China.

INTRODUCTION

Semiconductor photocatalysis technology, which provides a relatively simple method for the chemical conversion of solar energy, has received considerable attention because of its application for water splitting and the elimination of chemical contaminants.¹⁻³ Since Fujishima and Honda's paper of water splitting by TiO₂ under UV illumination firstly published in Nature in 1972,⁴ a variety of photocatalysts have been synthesized and used to convert solar energy into chemical energy to decompose materials into useful materials including hydrogen⁵⁻⁷ and hydrocarbons,⁸ as well as to remove pollutants and bacteria⁹⁻¹⁴ in air and water.^{15, 16} Nowadays TiO₂ is the most widely used photocatalyst because of its biological and chemical stability, non-toxicity, cost effectiveness and high activity.¹⁷⁻¹⁹ But TiO₂ can only utilize ultraviolet light due to its broad energy gap (3.2 eV) which will seriously restrict its applications, so finding photocatalysts that can utilize visible light has become the hot issue. Up to now a number of sulfides, nitrides and oxynitrides have been investigated as alternative materials for visible light or solar photocatalysis,²⁰⁻²³ especially transition-metal nanocrystalline chalcogenides which have attracted much attention over the past few years for their interesting properties and many potential applications.^{24, 25} Among them copper sulfide (CuS) is one of the most promising ones.

As an important transition-metal nanocrystalline chalcogenides and p-type semiconductor, CuS is one of the most intensively studied materials owing to its unusual electronic, optical, and other physical and chemical properties,²⁶⁻²⁹ and has great potential in a wide range of applications such as optical filters and superionic materials,³⁰ solar controller and solar radiation absorber,³¹ high-capacity cathode material in lithium secondary batteries,³² superconductor at low temperature,³³ and thermoelectric materials.³⁴ CuS nanoparticles with various morphologies, such as urchin-like structures,³⁵ nanoribbons,³⁶ nanowires,³⁷ microtubes,³⁸ nanoflowers³⁹ and

hollowspheres^{40,41}, have been synthesized via various approaches like solventless and solution thermolysis, sacrificial templating, solution phase reactions, hydrothermal or solvothermal method, ultrasonic and microwave irradiation, template-assisted methods, microemulsion, electrodeposition and chemical vapor deposition,⁴² many of which have shown prominent photocatalytic performances. Although most researches are mainly concerned with the synthesis of CuS with various stereoscopic structures, few investigations are focused on the controllable synthesis of two-dimensional nanostructures like nanodisks or nanoplates. In this work, we reported a simple and practical strategy for the controllable synthesis of a novel CuS two-dimensional microstructure composed of uniform nanodisks via a facile one-step solvothermal process at 150 °C for 2 h employing PVP as the surfactant. The phase, morphology evolution and optical properties were investigated with a special emphasis on the effects of S/Cu molar ratio ($x_{S/Cu}$) of raw materials and PVP content (x_{PVP}).

Experimental

Materials. Copper nitrate ($Cu(NO_3)_2$), thiourea ($CS(NH_2)_2$) and polyvinylpyrrolidone-K30 (PVP-K30) were selected as copper source, sulfur source and surfactant, respectively, while ethanediol was used as solvent. All chemical reagents used here were of analytical grade without any further purification.

Preparation of photocatalysts. In the typical synthesis process of CuS nanodisks, 3 mmol $Cu(NO_3)_2 \cdot 3H_2O$, 12 mmol $CS(NH_2)_2$ and 0.4 g PVP-K30 were introduced to 50 mL ethanediol with vigorous stirring and heating. The mixed solution was then transferred into a Teflon-lined stainless steel autoclave (100 mL capacity), sealed and maintained at 150 °C for 2 h. The resultant black solid product was filtered, washed with de-ionized water and ethanol for three times respectively and dried in the oven (DHG-9053A, Shanghai Yiheng Instruments Co., Ltd.,

China) at 60 °C. $x_{S/Cu}$ was controlled at 1, 2, 4 and 8 respectively by varying the content of $CS(NH_2)_2$ from 3 mmol to 24 mmol, while other conditions were kept at the typical synthesis. Besides, a changed x_{PVP} was applied at 0, 0.1, 0.2, 0.4 and 0.8 g in order to study the role played in the formation of nanodisks.

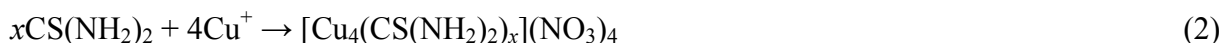
Characterization techniques. The phase structure was analyzed by X-ray diffraction (XRD: D/max-RB, Rigaku Inc., Japan) with a Cu $K\alpha$ radiation ($\lambda = 0.15406$ nm) filtered through a Ni foil. The morphologies of powders were observed by the field emission scanning electron microscopy (FESEM: SUPRATM 55, Carl Zeiss, Nakano, Japan) and transmission electron microscopy (TEM: Philip Tecnai F20, Dutch). The absorption spectra were measured by UV-visible spectrophotometer (UV-2800, UNICO Instruments Co., Ltd., China). The photocatalytic activities were evaluated by the degradation of RhB from Beijing Beihua Fine Chemical Co., Ltd., under visible-light irradiation using a 20 W Xe lamp (Beijing institute of electrical light sources, China) with a cutoff filter ($\lambda > 400$ nm). The photocatalytic decomposition of RhB by resultant powders was examined by the UV-visible spectrophotometer. In this experiment, 200 mL RhB solution (2.5 mg/L) was mixed with 0.01 g resultant powders and 0.2 mL of H_2O_2 (30%). The reaction temperature was kept at room temperature to prevent any thermal catalytic effect. The mixture was firstly placed in the dark to reach the adsorption/desorption equilibrium between photocatalysts and RhB before illumination, and then under constant vigorous stirring with the photoreactor during the photocatalytic process. The system was maintained at room temperature by circulation of water through an external cooling coil. At given intervals of illumination, ca. 5 mL of the mixture solution were taken out and centrifuged. After centrifugation, the UV/Vis spectrum of the supernatant was recorded to monitor the absorption behavior. Lambert-Beer's law indicates that the concentration of RhB

solution is in direct proportion to the absorption intensity of its UV-visible characteristic absorption peak. So the absorbance of the solution during photocatalysis process can be used as an index to characterize photocatalysts' efficiency of the dye's degradation. The degradation of RhB was monitored from the intensity of absorption peak of RhB (560 nm) relative to its initial intensity using the spectrophotometer under various illumination times on the basis of the following formula: $\eta = (A_0 - A_t) / A_0 \times 100\%$, where η , A_0 and A_t stand for the decolourization ratio of the reaction, the absorbance of RhB solution before and after reaction for t min, respectively.

Results and discussions

Figure 1 shows XRD patterns and FESEM images of samples prepared at different $x_{S/Cu}$ with a fixed x_{PVP} of 0.4 g by the typical solvothermal method. According to the XRD patterns, when $x_{S/Cu}$ is 1, all the diffraction peaks in Figure 1A (a) are well-matched with the pattern of the rhombohedral CuSCN phase (\diamond) (PDF#29-0581) without any detectable second phase. And from the EDS result (Figure S1 in Supporting Information), it can be found that the element composition of this sample is also approximately equal to that of CuSCN, which could further demonstrate the formation of CuSCN phase. As $x_{S/Cu}$ reaches to 2, CuS phase (∇) indexed by PDF#76-1725 begins to arise and becomes the main phase, along with four peaks attributable to (003), (101), (110) and (113) planes of CuSCN phase in the XRD patterns. When $x_{S/Cu}$ increases to 4 and further reaches 8, all the samples show a typical pattern of hexagonal CuS phase with a space group of $P6_3/mmc$ and unit cell dimension $3.8 \times 3.8 \times 16.4$ Å (PDF#76-1725). By using the Scherrer equation, $D = 0.9\lambda/\beta\cos\theta$, where λ is the X-ray wavelength, β is the full width at half maximum (FWHM), and θ is the diffraction angle, the mean diameter D of the CuS crystalline grains was estimated to be ca. 16.30 nm at $x_{S/Cu} = 4$ which further increases to 31.33 nm at $x_{S/Cu} = 8$ exerting an enhanced crystallinity with the increase of $x_{S/Cu}$.

In this experiment, as $\text{Cu}(\text{NO}_3)_2$ and $\text{CS}(\text{NH}_2)_2$ were introduced to the solution, a relatively stable complex $[\text{Cu}(\text{CS}(\text{NH}_2)_2)_x](\text{NO}_3)_4$ was initially formed in ethanediol at room temperature as described in eqs. (1-2).



When $x_{\text{S}/\text{Cu}} = 1$, the formation of CuSCN may be due to that NO_3^- ion is a better electron scavenger than other ions and can capture electrons (e^-) released by the reducing agent ($\text{CS}(\text{NH}_2)_2$). The free NO_3^- ions could accept e^- from $\text{CS}(\text{NH}_2)_2$ ions inducing the isomerization of $\text{CS}(\text{NH}_2)_2$ into ammonium thiocyanate (NH_4SCN) during the solvothermal process and NH_4SCN can further react with Cu^+ ions into CuSCN .⁴³ The reaction process can be depicted through the following eqs. (3-4):



In the case of $x_{\text{S}/\text{Cu}} \geq 1$, the complex $[\text{Cu}(\text{CS}(\text{NH}_2)_2)_x](\text{NO}_3)_4$ was also initially formed in ethanediol at room temperature as described in eq. (1-2). However, the isomerization of $\text{CS}(\text{NH}_2)_2$ into NH_4SCN during the solvothermal process and the formation of CuSCN reacted between NH_4SCN and Cu^+ ions in eqs. (3-4) would be disturbed as the increase of $\text{CS}(\text{NH}_2)_2$ in the system. When the reactive temperature was raised to a moderate solvothermal degree of ca. 150 °C, the excess $\text{CS}(\text{NH}_2)_2$ induces Cu^+ into Cu^{2+} during its release of S^{2-} which reduces the reactive opportunity of Cu^+ ions with NH_4SCN into CuSCN (eq. 4). Both further facilitate the formation of CuS phase as depicted speculatively in eq. (5):



Hence, the increase of $\text{CS}(\text{NH}_2)_2$ in the system also leads to the relative decrease of free Cu^{2+} and/or Cu^+ ions during the product precipitation process, which will lower the supersaturation of precursor solution to reduce the nucleation rate of CuS particles and promote the growth of the particles into the micrometer size regime.⁴⁴ Consequently, CuS particles tend to grow into larger structures in the case of higher $x_{\text{S}/\text{Cu}}$. The detail mechanism for the formation of different morphologies still needs further investigation.

Apart from changed phase pattern in Figure 1A, obviously different morphologies are noticed in the synthetic products depending on $x_{\text{S}/\text{Cu}}$ as shown in FESEM images in Figure 1B-E. When $x_{\text{S}/\text{Cu}}$ is 1, the sample is mainly composed of many large irregular particles with the size of ca. 5 μm along with dispersed small ones (Figure 1B). Besides, as shown in the inset of Figure 1B the small ones are around 500 nm in diameter and built up by many nanoplates. As $x_{\text{S}/\text{Cu}}$ increases to 2, the sample is composed of many nanoparticles similar to that shown in the inset of Figure 3B, but the average particle size shrinks to ca. 400 nm, which is attributed to the arising of second phase (CuS) in the system. When $x_{\text{S}/\text{Cu}}$ further increases to 4, the resultant powders grow into many uniform nanodisks with an average diameter and thickness of ca. 500 nm and 50 nm, respectively, as shown in Figure 1D. Besides, CuS nanodisks are heaped up by many much smaller nanosheets with a concentrated particle size distribution between 400 nm and 600 nm as shown in the inset (a) and (b) of Figure 1D, respectively. With $x_{\text{S}/\text{Cu}}$ increasing to 8, the nanodisks, compared with those prepared at $x_{\text{S}/\text{Cu}} = 4$, thicken markedly and show a tendency of self-assembly into concaved cuboctahedral superstructures (inset of Figure 1E), which is similar to that reported by Chunyan Wu et al.⁴⁵ The novel uniformly dispersed nanodisk structure obtained at $x_{\text{S}/\text{Cu}} = 4$ is rarely reported so far and from the full nitrogen sorption isotherms (see Supporting Information, Figure S2) the specific surface area was evaluated to be $13.017 \text{ m}^2 \cdot \text{g}^{-1}$

from data points in this pressure range by the BET equation. So this novel structure may have potential applications in the field of p-type semiconductor, sensor, solar energy converter, cathode material, catalyst, optical filter, and nonlinear optical material.

In order to further understand the morphologies and nanostructures of the CuS nanodisks prepared at $x_{S/Cu} = 4$ and $x_{PVP} = 0.4$ g, the TEM and HRTEM (short for high resolution transmission electron) analysis were applied. As shown in Figure 2A the nanodisk with an average diameter of ca. 500 nm is well in accordance with those provided by FESEM. Many well arranged stripes distributing on the nanodisk are also observed in which the included angle of stripes at different directions are fixed at ca. 120° . These stripe patterns are Moire' fringes which originated from the superimposition of two oblique CuS superlattices with the longer base vector in common⁴⁶. And fixed included angle (ca. 120°) indicates that the CuS grains at the same layer were well aligned making it difficult to detect the grain boundaries. So there is no obvious boundary observed in the given field of view (ca. 45×45 nm) of the corresponding HRTEM image in Figure 2B. As a consequence, the HRTEM image cannot accurately reflect the average grain size of ca. 16.30 nm calculated from XRD. According to the SAED patterns (Figure 2C) the nanodisks are polycrystalline, which further proves their self-assembling of many small CuS crystal particles. Along with a schematic sketch of the CuS unit cell shown in the insert of Figure 2E, the HRTEM image and its FFT ED (short for fast Fourier transformation electric diffraction) pattern in Figure 2E and D clearly show a lattice spacing of 0.19 nm, which are consistent with the distance between the $\{110\}$ lattice planes of CuS phase, indicating that the CuS nuclei crystallize radially along $\{001\}$ planes and further compact into nanodisk structures.

Since PVP addition played a key role on the synthesis of CuS nanodisks, the effect of the content was also studied in detail while other conditions were fixed at the typical synthesis.

structures had already formed with an average particle size of 440 nm and further grew to ca. 540 nm between 30 min and 60 min. The assembling of CuS nanodisks had finished in the first 60 min of the reaction, after that there was little change to the nanodisks and the average particle size kept at 530-540 nm, which also aptly indicates the short time consuming and controllability of our synthetic method.

Furthermore, a schematic mechanism diagram related to the formation process of CuS nanodisks is proposed and displayed in Figure 5. When $\text{Cu}(\text{NO}_3)_2$, $\text{CS}(\text{NH}_2)_2$ and PVP were introduced to the solution $[\text{Cu}(\text{CS}(\text{NH}_2)_2)_x](\text{NO}_3)_4$ was initially formed in ethanediol at room temperature. During this process PVP uniformly dispersed around the complex without reacting with it since no change such as precipitation or color change happened to the solution after adding PVP. When the reactive temperature was raised to a moderate solvothermal degree of ca. 150 °C the as-formed complex decomposed into CuS nuclei whose reaction equations have already been depicted in eqs. (1), (2) and (5). Driven by the characteristic of hexagonal structure of CuS, the as-formed CuS nuclei then aggregated together and recrystallized into plate crystals with many PVP molecules adsorbed on the surface functioning as potential crystal face inhibitors in the system which benefit the formation of oriented nucleation.⁵⁰ Owing to the minimization of surface free energy in this system, the as-formed plate crystals would further aggregate with each other into nanodisks.⁵¹ As shown in Figures. 3A-E, the downward tendency of the particle size with further addition of PVP can be ascribed to the “coating effect” of PVP, in which the excess PVP forms coating layers on CuS nanodisks that inhibit the further grains aggregation.

The optical absorption properties of the as-prepared nanopowders were investigated with an emphasis on their morphologies and phase structures. Figure 6A shows the optical absorption spectra of nanopowders prepared at different conditions. When $x_{\text{S}/\text{Cu}} = 1$, the CuSCN particles'

(sample a) absorption peaks are mainly located at 300 nm and 830 nm which are within the ultraviolet and infrared regions belonging to the intrinsic band-gap absorption of CuSCN. As $x_{S/Cu}$ rises to 2, apart from the absorption peaks remaining at 300 nm, the peak in infrared region exerts a red-shift to 800 nm which is attributed to the appearance of CuS phase in mixture of CuSCN and CuS (sample b). As to CuS nanodisks, CuS concaved cuboctahedral superstructures and CuS nest-like structures (samples c-e), because they are composed of CuS phase which has been shown in the XRD patterns, their absorption peaks exert intrinsic band-gap absorption of CuS located at 370 nm and 650 nm. Besides, the CuS concaved cuboctahedral superstructures (sample d) and CuS nest-like structures (sample e) have stronger absorptions in the visible region which result from cavity-mirror effect of CuS hierarchical structure as shown in the inset of Figure 6A. When the wavelength of light is close to the size of cavities, photoabsorption can be enhanced by reflected many times among the nanoplates which serve as “mirrors”. In our case, CuS superstructures with a size of ca. 1 μm serve as excellent light-cavity mirrors of visible light, which leads to a great enhancement of the reflection and absorption ability for light.^{52, 53} According to optical absorption spectra, all the samples composed of CuS phase have spectral responses in visible-light region indicating a potential in utilization of visible light during photocatalytic process.

To further understand the behavior of the optical absorption, the energy band gap (E_g) was estimated based on Tauc equation: $\alpha h\nu = A (h\nu - E_g)^m / h\nu$, where m is an index which determines the type of optical transition ($m = 2$ and $1/2$ corresponding to indirectly allowed and directly allowed, respectively), and A , E_g and $h\nu$ are a constant, the optical band gap energy and the incident photon energy, respectively. When $m = 2$, E_g is negative by extrapolating the linear region of the curve to the $h\nu$ axis where $(\alpha h\nu)^2 = 0$ (not shown here), while E_g could be

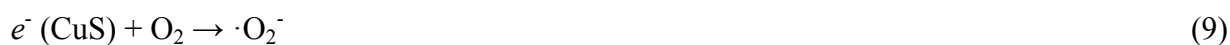
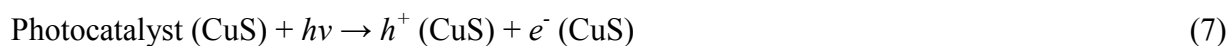
calculated as 2.03 eV, 2.19 eV, 1.75 eV, 1.54 eV and 1.64 eV for the CuSCN particles (a), mixture of CuSCN and CuS (b), CuS nanodisks (c), CuS concaved cuboctahedral superstructures (d) and CuS nest-like structures (e), respectively, as shown in Figure 6B, by the same approach as $m = 1/2$, which confirms CuS and CuSCN are all direct band gap semiconductors.

The photocatalytic activities of the as-prepared samples were evaluated by measuring the degradation of RhB in an aqueous solution under visible light and the time-dependent absorption spectra of RhB solutions under visible light illumination in the presence of different photocatalysts are first shown in Figure 7A-E. As can be seen from the five spectra, the absorbance of RhB in CuSCN and CuSCN/CuS suspensions changes slowly and only ca. 45.54% and 50% of RhB are degraded in 120 min (Figure 7A and B). This is due to the wide E_g and low photocatalytic activity of CuSCN phase, but it is obvious that the arising of CuS phase in CuSCN system can to some extents improve the photocatalytic performance of mixed-phase nanopowders. This enhanced performance may be ascribed to the formation of heterostructure between CuS and CuSCN, which can reduce the electron-hole (e^-h^+) combination rate. However, nanodisks with a CuS phase show a sharp decrease in RhB absorption at 553 nm in the photodegradation, indicating an excellent photocatalytic performance which can degraded 93.23% of the RhB solution in 120 min (Figure 7C). CuS self-assembled superstructures show a slightly lower the degradation rate of RhB than that of the nanodisks reaching 85.65% in 120 min (Figure 7D). This can be ascribed to the increased particle size which can extend the distance for photoinduced e^-h^+ to travel to the surface of the particles resulting in an increase of combination rate.¹⁶ As CuS phase changes to nest-like structure the photocatalytic activity continues to decline, only 58.88% of RhB are degraded in 120 min (Figure 7E). This is due to the fiercely growing particle size of samples which can lead to a lower absorption rate of RhB

molecules to the photocatalysts, so as to exert an inferior absorption behavior during the dark treatment (curve e) as shown in Figure 7F.

The photocatalytic activities of different catalysts in the degradation of RhB under visible light irradiation are compared in Figure 7F. It can be clearly found that the blank group (f) in which only 0.2 mL of H₂O₂ were added shows the lowest photocatalytic activity and only 37.84% of RhB can be degraded in 120 min. Besides, the introduction of the CuSCN particles (a), mixture of CuSCN and CuS (b) and CuS nest-like structures (e) only bring a slight promotion to the photocatalytic rate of RhB. However, the introduction of CuS nanodisks (c) and CuS concaved cuboctahedral superstructures (d) can improve significantly the degradation of RhB, especially CuS nanodisks which exert outstanding photocatalytic activity during the whole catalytic process indicating an excellent photocatalytic performance of CuS nanodisks.

The generally accepted major reaction steps related to the photocatalytic mechanism of CuS semiconductors are summarized by eqs. (7-12) as well as shown in schematic illustration in Figure 8A.



When CuS sample is irradiated under visible light, e^- are excited from the valence band to the conduction band of CuS particles as the absorption of photon energy is greater than or equal to E_g of CuS, leaving h^+ in the same spot where the excitation of e^- occurs. These photogenerated

e^- and h^+ then transfer to the surface of CuS particles and react with oxidants and reductants, respectively. Generally, photogenerated e^- are expected to be trapped by O_2 in the solution to form superoxide ions ($\cdot O^{2-}$) and/or other reactive oxygen species. The water (H_2O) in RhB solution is split into hydrogen ions (H^+) and hydroxyl ions (OH^-), and h^+ are induced to react with OH^- accordingly in RhB solution to produce hydroxyl free radicals ($\cdot OH$) and other free radicals with strong oxidation.^{17, 54} These separated reactive oxygen species and free radicals can participate in the photocatalytic reactions to decompose organic compounds such as RhB. In this study, CuS nanodisks have a two-dimensional structure which can significantly reduce the distance for photoinduced e^- - h^+ to travel to the surface and inhibit their recombination. Ascribed to the quantum size effect the uniform flaky units have a good adsorption rate of RhB molecules which promotes the photocatalytic reactions. So CuS nanodisks exert excellent photocatalytic performance among all photocatalysts. Furthermore, as shown in Figure 8B, monodispersed CuS nanodisks prepared in our work also exert superior performance indicating a promising application prospect compared with CuS and commercial P25 photocatalysts reported by other researchers.⁵⁵⁻⁵⁸ In the practical application, stability is very essential, so in order to prove the stability of CuS nanodisks, XRD testing of the powders was carried out before and after the photocatalytic reaction. From the XRD patterns (see Supporting Information, Figure S3), it can be found that the phase composition remains CuS (PDF#76-1725) during the reactions indicating the good chemical stability of samples in the photocatalytic process.

Conclusions

Uniform CuS nanodisks with ca. 500 nm in diameter have been successfully synthesized by a facile solvothermal method at 150 °C for 2 h employing PVP as the surfactant. $x_{S/Cu}$ affects the phase structure and morphology of the product, and a pure CuS phase shaped in nanodisks was

obtained as $x_{S/Cu} = 4$, on which x_{PVP} has little effect on pure CuS phase of nanodisks despite a refined slightly diameter of nanodisks from 636 nm to 456 nm. CuS nanodisks are compacted with many grains of about 16-22 nm that crystallize radially along {001} planes. The optical absorption properties of resultant powders depend greatly on phase compositions and morphologies, in which a broad absorption in the visible region was observed in all the products with a CuS phase. The CuS nanodisks with a bandgap of 1.75 eV exerted an excellent photocatalytic performance, which degraded over 93.23% of RhB in 2 h under visible-light (> 400 nm) irradiation.

Acknowledgments

This work was supported by National Natural Science Foundation of China (Grant No. 51272023), National Basic Research Program of China (Grant No. 2013CB632500).

References

1. M. Anpo, S. Dohshi, M. Kitano, Y. Hu, M. Takeuchi and M. Matsuoka, *Ann. Rev. Mater. Res.*, 2005, **35**, 1.
2. G. Hitoki, T. Takata, J.N. Kondo, M. Hara, H. Kobayashi and K. Domen, *Electrochemistry*, 2002, **70**, 463.
3. Y. Tian and T. Tatsuma, *J. Am. Chem. Soc.*, 2005, **127**, 7632.
4. A. Fujishima and K. Honda., *Nature*, 1972, **238**, 37.
5. A. Kudo and Y. Miseki, *Chem. Soc. Rev.*, 2009, **38**, 253.
6. K. Maeda, *J. Photochem. Photobiol. C*, 2011, **12**, 237.

7. A. Ryu, *J. Photochem. Photobiol. C*, 2010, **11**, 179.
8. T. Inoue, A. Fujishima, S. Konishi and K. Honda, *Nature*, 1979, **277**, 637.
9. L. Caballero, K.A. Whitehead, N.S. Allen and J. Verran, *J. Photochem. Photobiol. A*, 2009, **202**, 92.
10. R. Cai, K. Hashimoto, K. Itoh, Y. Kubota and A. Fujishima, *Bull. Chem. Soc. Japan*, 1991, **4**, 1268.
11. T. Matsunaga, R. Tomoda, T. Nakajima and H. Wake, *FEMS Microbiol. Lett.*, 1985, **29**, 211.
12. C. McCullagh, J. Robertson, D. Bahnemann and P. Robertson, *Res. Chem. Intermed.*, 2007, **33**, 359.
13. J.R. Peller, R.L. Whitman, S. Griffith, P. Harris, C. Peller and J. Scalzitti, *J. Photochem. Photobiol. A*, 2007, **186**, 212.
14. E.J. Wolfrum, J. Huang, D.M. Blake, P. Maness, Z. Huang, J. Fiest and W.A. Jacoby, *Environ. Sci. Technol.*, 2002, **36**, 3412.
15. J. Zhao, B. Zhang, Y. Li, L. Yan and S. Wang, *J. Alloy. Compd.*, 2012, **535**, 21.
16. S. Li, Y. Lin, B. Zhang, J. Li and C. Nan., *J. Appl. Phys.*, 2009, **105**, 054310.
17. M.R. Hoffmann, S. T. Martin, W.Y. Choi and D.W. Bahnemann, *Chem. Rev.*, 1995, **95**, 69.
18. A. L. Linsebigler, G. Q. Lu and J. T. Yates, *Chem. Rev.*, 1995, **95**, 735.
19. K. Su, Z. H. Ai and L. Z. Zhang, *J. Phys. Chem. C*, 2012, **116**, 17118.

20. F.E. Osterloh., *Chem. Mater.*, 2008, **20**, 35.
21. H. Shao, X. Qian and Z. Zhu, *J. Solid State Chem.*, 2005, **178**, 3522.
22. P.S. Lunawat, S. Senapati, R. Kumar and N.M. Gupta, *Int. J. Hydrogen Energy*, 2007, **32**, 2784.
23. J.S. Jang, U.A. Joshi and J.S. Lee., *J. Phys. Chem. C*, 2007, **111**, 13280.
24. Y. Liu, P.D. Kanhere, C.Ling. Wong, Y. Tian, Y. Feng, F. Boey, T. Wu, H. Chen, T.J. White, Z. Chen and Q. Zhang, *J. Solid State Chem.*, 2010, **183**, 2644.
25. B.B. Kale, J.O. Baeg, S.M. Lee, H. Chang, S.J. Moon and C.W. Lee, *Adv. Funct. Mater.*, 2006, **16**, 1349.
26. R. Córdova, H. Gómez, R. Schrebler, P. Cury, M. Orellana, P. Grez, D. Leinen, J.R.Ramos-Barrado and R.D. Río, *Langmuir*, 2002, **18**, 8647.
27. W.P. Lim, C.T. Wong, S.L. Ang, H.Y. Low and W.S. Chin, *Chem. Mater.*, 2006, **18**, 6170.
28. S. Erokhina, V. Erokhin, C. Nicolini, F. Sbrana, D. Ricci and E.D. Zitti, *Langmuir*, 2003, **19**, 766.
29. S. Gorai, D. Ganguli and S. Chaudhuri, *Cryst. Growth Des.*, 2005, **5**, 875.
30. L.F. Chen, W. Yu and Y. Li, *Powder Technol.*, 2009, **191**, 52.
31. F. Li, T. Kong, W.T. Bi, D.C. Li, Z. Li and X.T. Huang, *Appl. Surf. Sci.*, 2009, **255**, 6285.
32. J.S. Chung and H.J. Sohn, *J. Power Sources*, 2002, **108**, 226.
33. G.Z. Mao, W.F. Dong, D.G. Kurth and H. Möhwald, *Nano Lett.*, 2004, **4**, 249.

34. X.P. Shen, H. Zhao, H.Q. Shu, H. Zhou and A.H. Yuan, *J. Phys. Chem. Solids*, 2009, **70**, 422.
35. L.Y. Zhu, Y. Xie, X.W. Zheng, X. Liu and G.E. Zhou, *J. Cryst. Growth*, 2004, **260**, 494.
36. C.H. Tan, R. Lu, P.C. Xue, C.Y. Bao, Y.Y. Zhao, *Mater. Chem. Phys.*, 2008, **112**, 500.
37. J. Mao, Q. Shu, Y. Wen, H. Yuan, D. Xiao and M.M. Choi, *Cryst. Growth Des.*, 2009, **9**, 2546.
38. Z. Yao, X. Zhu, C. Wu, X. Zhang and Y. Xie, *Cryst. Growth Des.*, 2007, **7**, 1256.
39. T.Y. Ding, M.S. Wang, S.P. Guo, G.C. Guo and J.S. Huang, *Mater. Lett.*, 2008, **62**, 4529.
40. X. Meng, G. Tian, Y. Chen, R. Zhai, J. Zhou, Y. Shia, X. Cao, W. Zhou and H. Fu, *CrystEngComm*. 2013, **15**, 5144.
41. H. Zhu, J. Wang, D. Wu, *Inorg. Chem.*, 2009, **48**, 7099.
42. M. Basu, A.K.Sinha, M. Pradhan, S. Sarkar, Y. Negishi, and T. Pal, *Environ. Sci. Technol.*, 2010, **44**, 6313.
43. Z. Fang, C. Wang, F. Fan, S. Hao, L. Long, Y. Song and T. Qiang, *Chin. J. Chem*, 2013, **31**, 1015.
44. Q. Zhang, S.J. Liu and S.H. Yu, *J. Mater. Chem.*, 2009, **19**, 191.
45. C. Wu, S.H. Yu and M. Antonietti, *Chem. Mater.*, 2006, **18**, 3599.
46. W. Shenton, D. Pum, U.B. Sleytr and S. Mann, *Nature*, 1997, **389**, 585.
47. Y. Zhang, B. Zhang, Z. Ge, L. Zhu and Y. Li, *Eur. J. Inorg Chem.*, 2014, **2014**, 2368.

48. Z. Chen, Y. Tang, L. Zhang and L. Luo, *Electrochim. Acta*, 2006, **51**, 5870.
49. Z. Zhang, B. Zhao and L. Hu, *J. Solid State Chem.*, 1996, **121**, 105.
50. J. Wu, F. Duan, Y. Zheng and Y. Xie., *J. Phys. Chem. C*, 2007, **111**, 12866.
51. H. Qi, J.F. Huang, L.Y. Cao, J.P. Wu and D.Q. Wang, *Ceram. Int.*, 2012, **38**, 2195.
52. D. Wu, J. Duan, C. Zhang, K. Guo and H. Zhu, *J. Phys. Chem. C*, 2013, **117**, 9121.
53. Q. Tian, M. Tang, Y. Sun, R. Zou, Z. Chen, M. Zhu, S. Yang, J. Wang, J. Wang, J. Hu, *Adv. Mater.*, 2011, **23**, 3542.
54. S.S. Soni, M.J. Henderson, J.F. Bardeau and A. Gibaud, *Adv. Mater.*, 2008, **20**, 1493.
55. F. Li, J. Wu, Q. Qin, Z. Li and X. Huang, *Powder Technol.*, 2010, **198**, 267.
56. F. Li, W. Bi, T. Kong and Q. Qin, *Cryst. Res. Technol.*, 2009, **44**, 729.
57. K.V. Subba Rao, M. Subrahmanyam and P. Boule, *Environ. Technol.* 2003, **24**, 1025.
58. S. Yang, Y. Xu, Y. Cao, G. Zhang, Y. Sun and D. Gao, *RSC Adv.*, 2013, **3**, 21994.

Figure Captions:

Figure 1. XRD patterns (A) and FESEM images (B-D) of samples prepared at different $x_{S/Cu}$ with a fixed x_{PVP} of 0.4 g. (a, B) $x_{S/Cu} = 1$; (b, C) $x_{S/Cu} = 2$; (c, D) $x_{S/Cu} = 4$; (d, E) $x_{S/Cu} = 8$.

Figure 2. TEM (A), SAED (C), HRTEM (B, E) and FFT ED (D) images of CuS nanodisks prepared at the typical condition along with a schematic sketch of CuS unit cell (Inset of E shows a schematic sketch of the CuS unit cell).

Figure 3. FESEM images (A-D), XRD patterns (F), Grain and particle size variation trends (E) of samples prepared at different x_{PVP} with a fixed $x_{S/Cu}$ of 4. (A, a) $x_{PVP} = 0$ g; (B, b) $x_{PVP} = 0.1$ g; (C, c) $x_{PVP} = 0.2$ g; (D, d) $x_{PVP} = 0.8$ g.

Figure 4. FESEM images (A-E) and average particle sizes (F) of samples prepared by solvothermal method at the $x_{S/Cu}$ of 4 with $x_{PVP} = 0.4$ g for different holding times (A-30 min; B-60 min; C-90 min; D-120 min; E- 240 min).

Figure 5. Schematic forming mechanism diagram of CuS nanodisks.

Figure 6. Optical absorption spectra (A) and Plots of the $(ah\nu)^2$ vs. photon energy ($h\nu$) (B) for nanopowders with different morphologies and phase structures: a-the CuSCN particles; b-mixture of CuSCN and CuS; c-CuS nanodisks; d-CuS concaved cuboctahedral superstructures; e-CuS nest-like structures.

Figure 7. UV-vis absorption spectra changes of RhB aqueous solution in the presence of different photocatalysts(A-E) and photocatalytic efficiencies of different catalysts (F): A & a-the CuSCN particles; B & b-mixture of CuSCN and CuS; C & c-CuS nanodisks; D & d-CuS concaved cuboctahedral superstructures; E & e-CuS nest-like structures; f-blank group.

Figure 8. Schematic illustration of mechanism for the photocatalysis in CuS nanopowders under visible light irradiation (A) and comparison of photocatalytic performances of samples reported in other research (B).

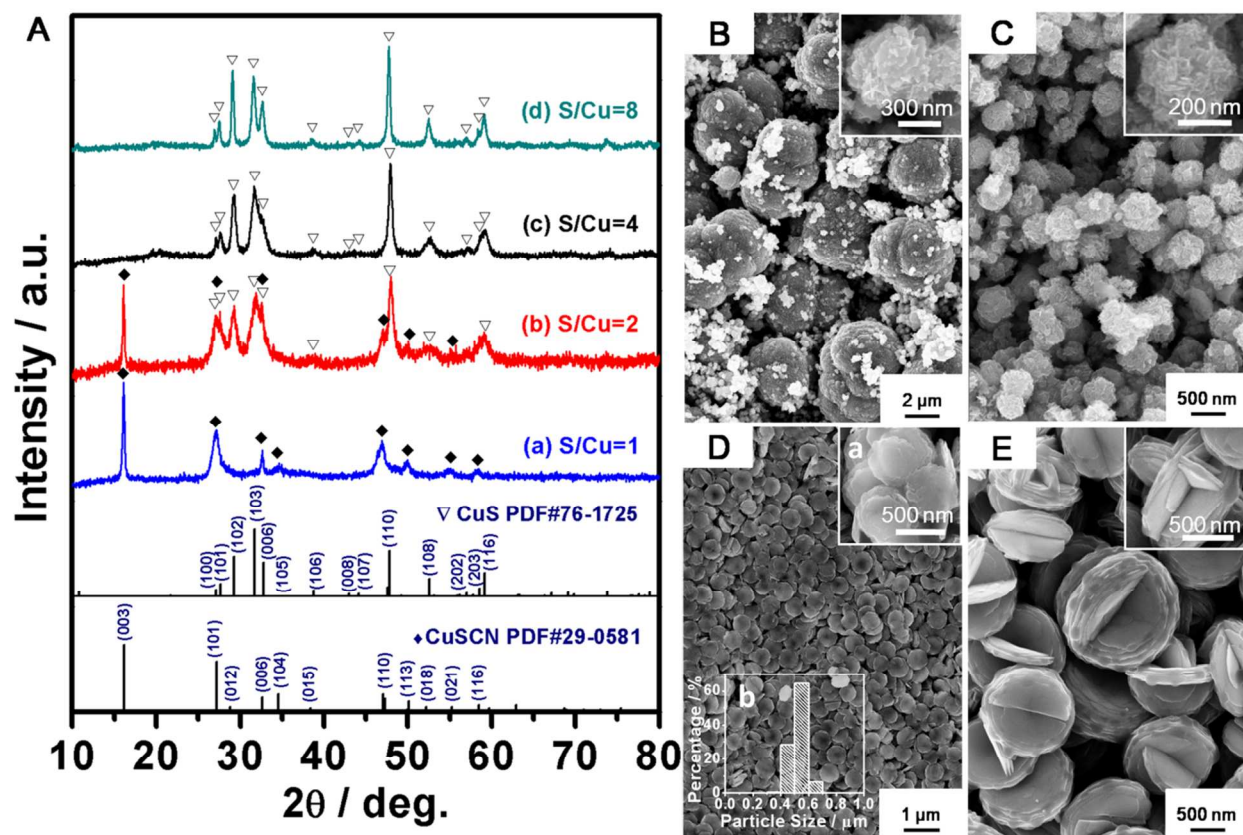


Figure 1. XRD patterns (A) and FESEM images (B-D) of samples prepared at different $x_{S/Cu}$ with a fixed x_{PVP} of 0.4 g. (a, B) $x_{S/Cu} = 1$; (b, C) $x_{S/Cu} = 2$; (c, D) $x_{S/Cu} = 4$; (d, E) $x_{S/Cu} = 8$.

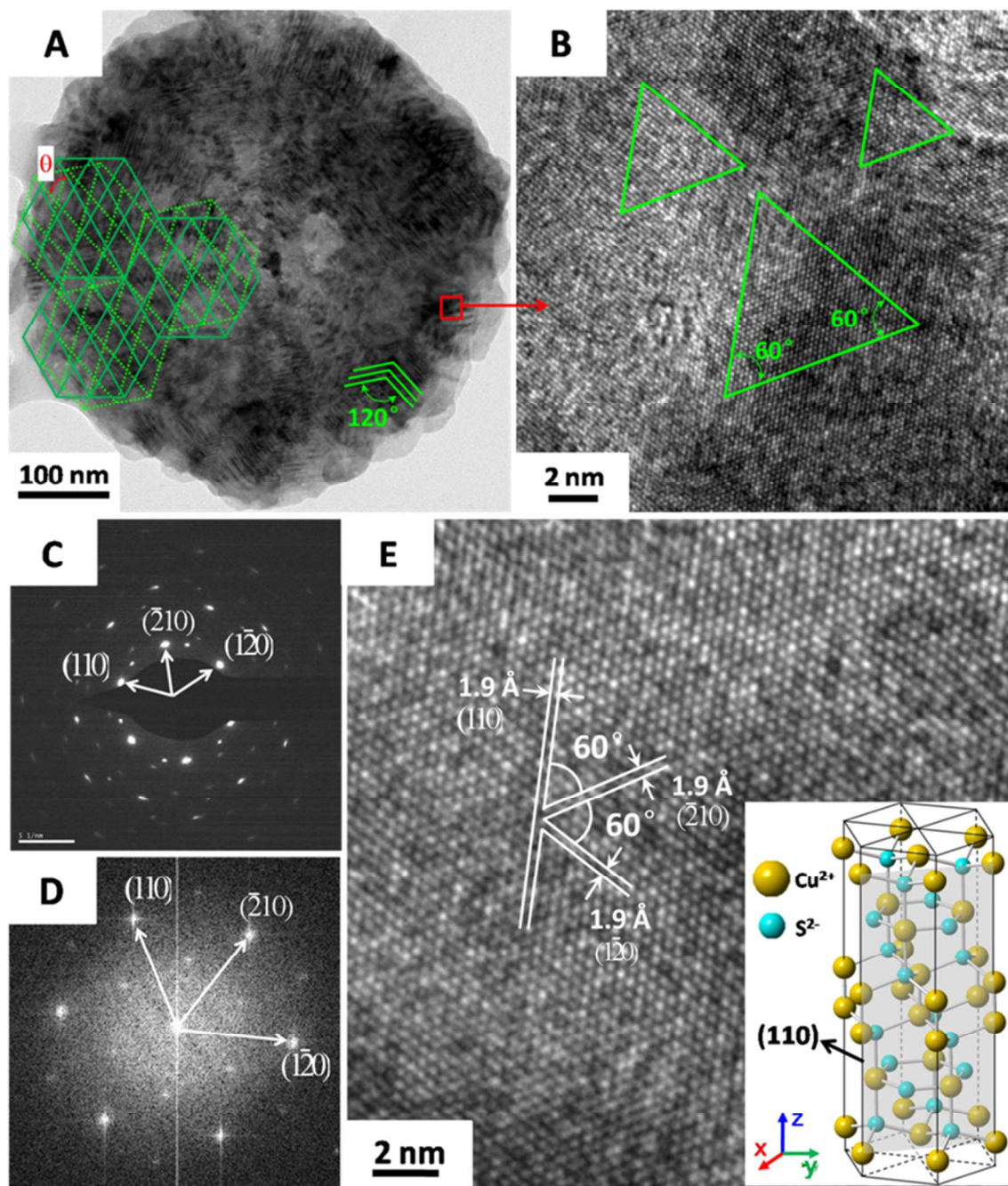


Figure 2. TEM (A), SAED (C), HRTEM (B, E) and FFT ED (D) images of CuS nanodisks prepared at the typical condition along with a schematic sketch of CuS unit cell (Inset of E shows a schematic sketch of the CuS unit cell).

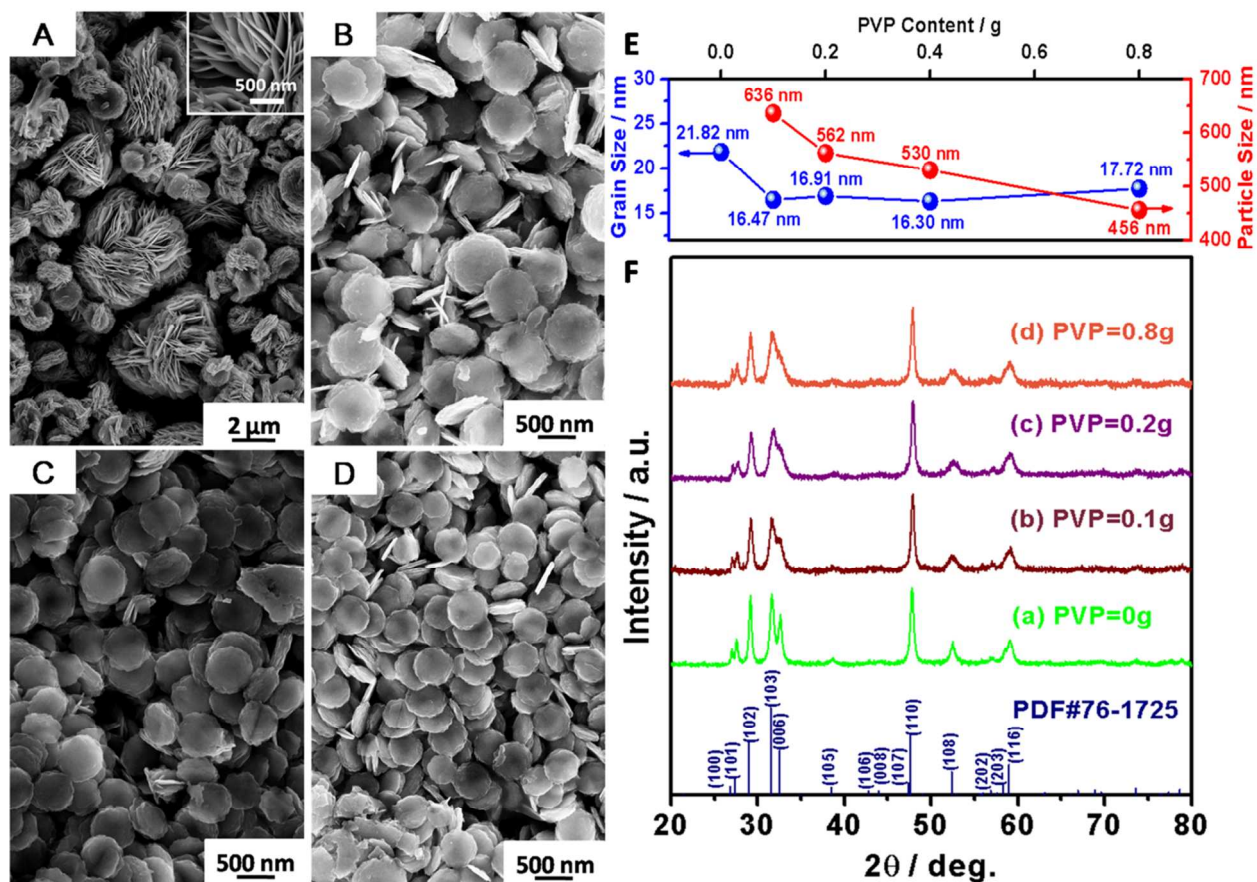


Figure 3. FESEM images (A-D), XRD patterns (F), Grain and particle size variation trends (E) of samples prepared at different x_{PVP} with a fixed $x_{\text{S/Cu}}$ of 4. (A, a) $x_{\text{PVP}} = 0$ g; (B, b) $x_{\text{PVP}} = 0.1$ g; (C, c) $x_{\text{PVP}} = 0.2$ g; (D, d) $x_{\text{PVP}} = 0.8$ g.

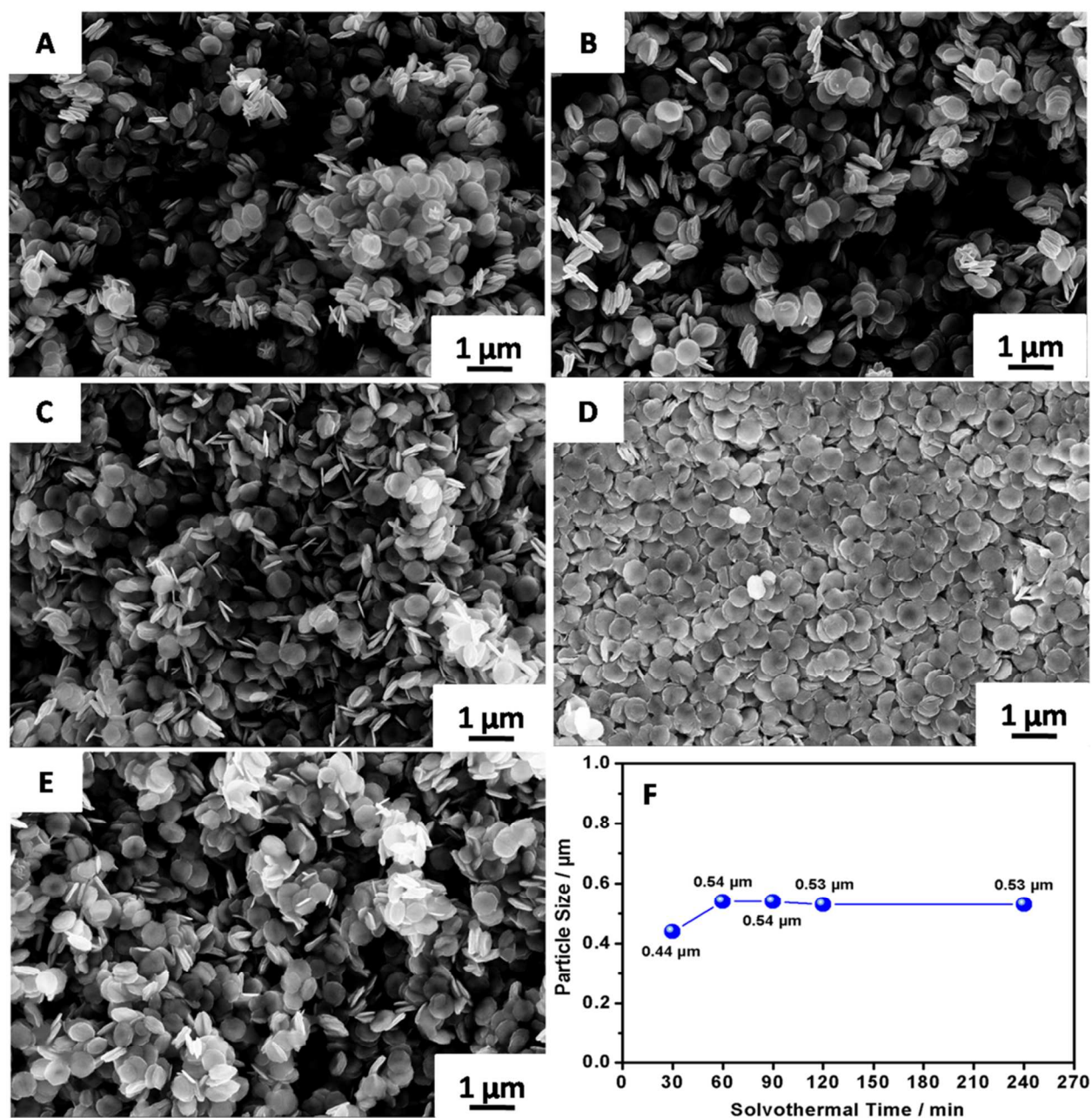


Figure 4. FESEM images (A-E) and average particle sizes (F) of samples prepared by solvothermal method at $x_{S/Cu}=4$ with $x_{PVP} = 0.4$ g for different holding times (A-30 min; B-60 min; C-90 min; D-120 min; E- 240 min).

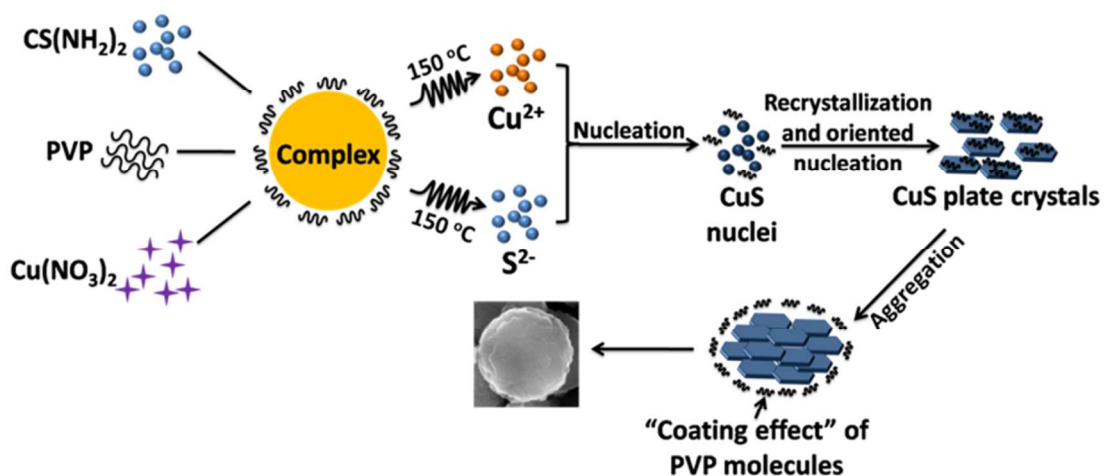


Figure 5. Schematic forming mechanism diagram of CuS nanodisks.

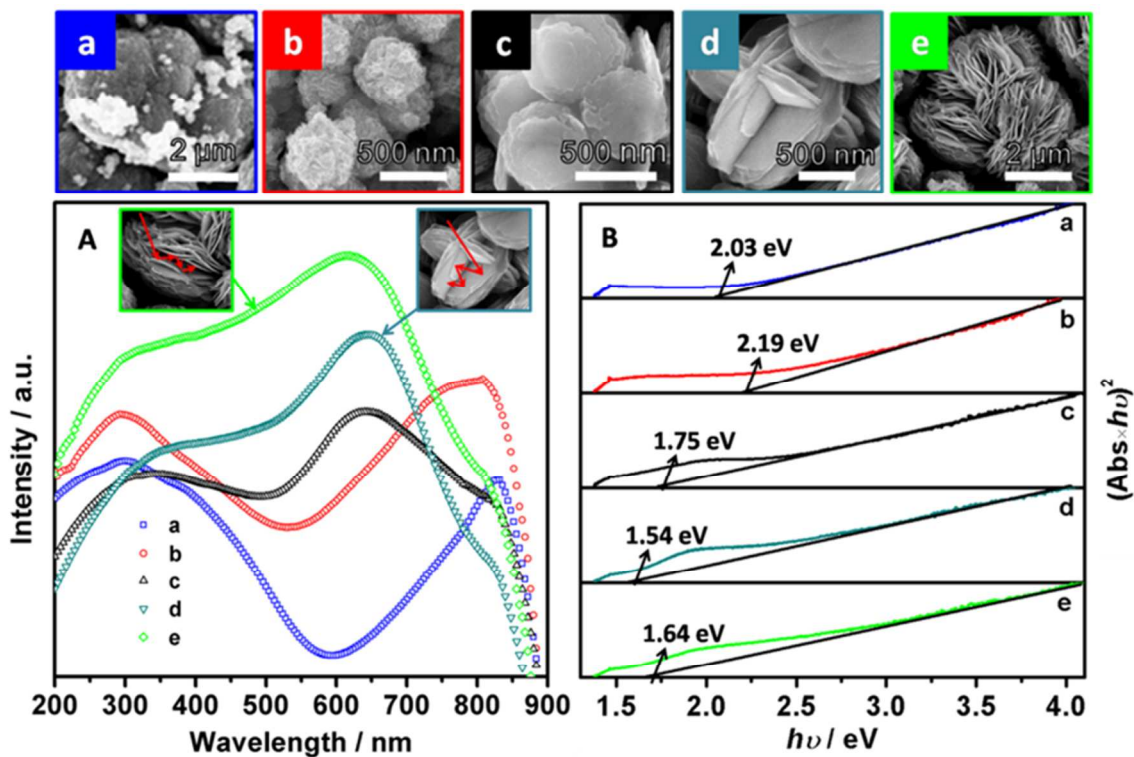


Figure 6. Optical absorption spectra (A) and Plots of the $(ahv)^2$ vs. photon energy (hv) (B) for nanopowders with different morphologies and phase structures: a-the CuSCN particles; b-mixture of CuSCN and CuS; c-CuS nanodisks; d-CuS concaved cuboctahedral superstructures; e-CuS nest-like structures.

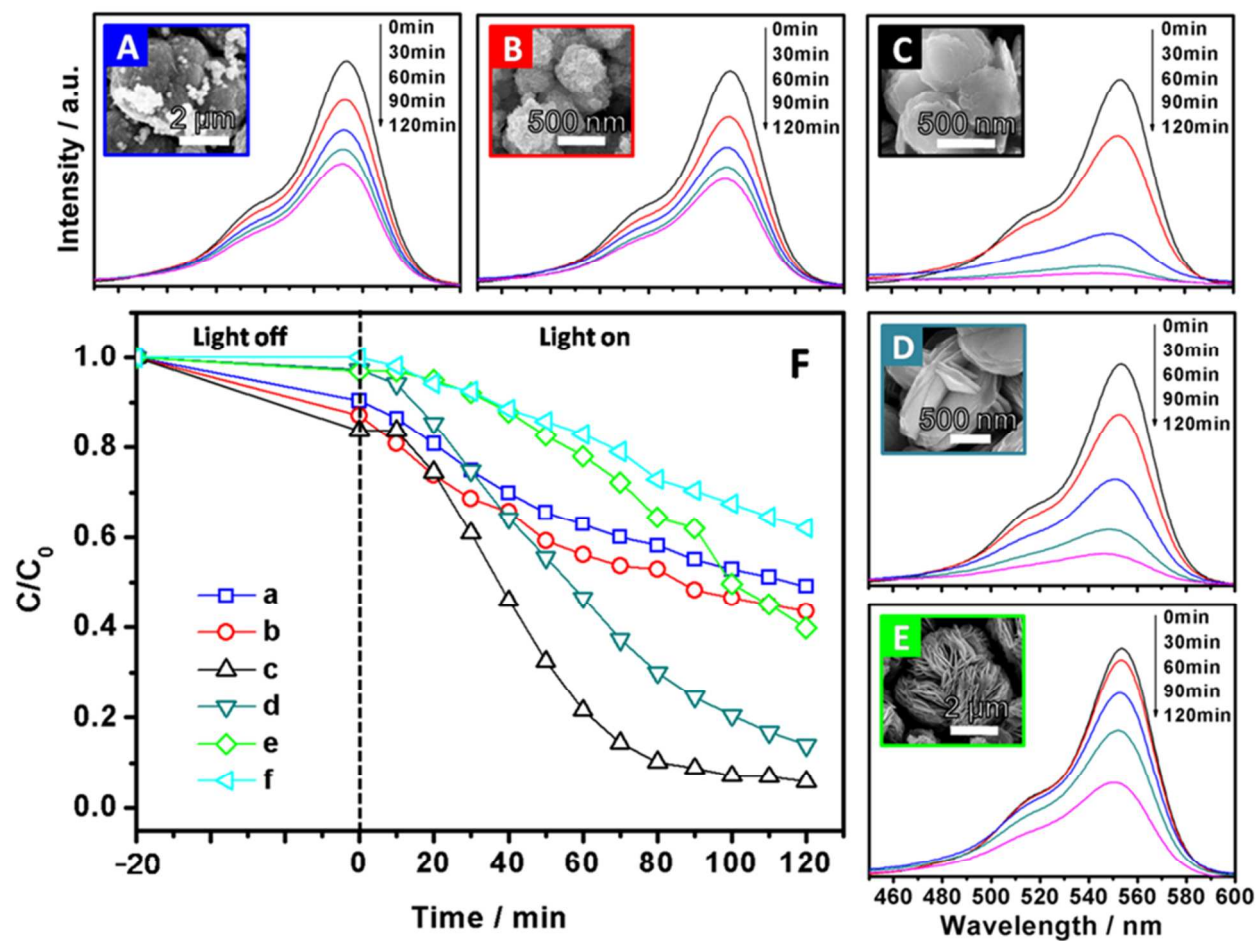


Figure 7. UV-vis absorption spectra changes of RhB aqueous solution in the presence of different photocatalysts(A-E) and photocatalytic efficiencies of different catalysts (F): A & a-the CuSCN particles; B & b-mixture of CuSCN and CuS; C & c-CuS nanodisks; D & d-CuS concaved cuboctahedral superstructures; E & e-CuS nest-like structures; f-blank group.

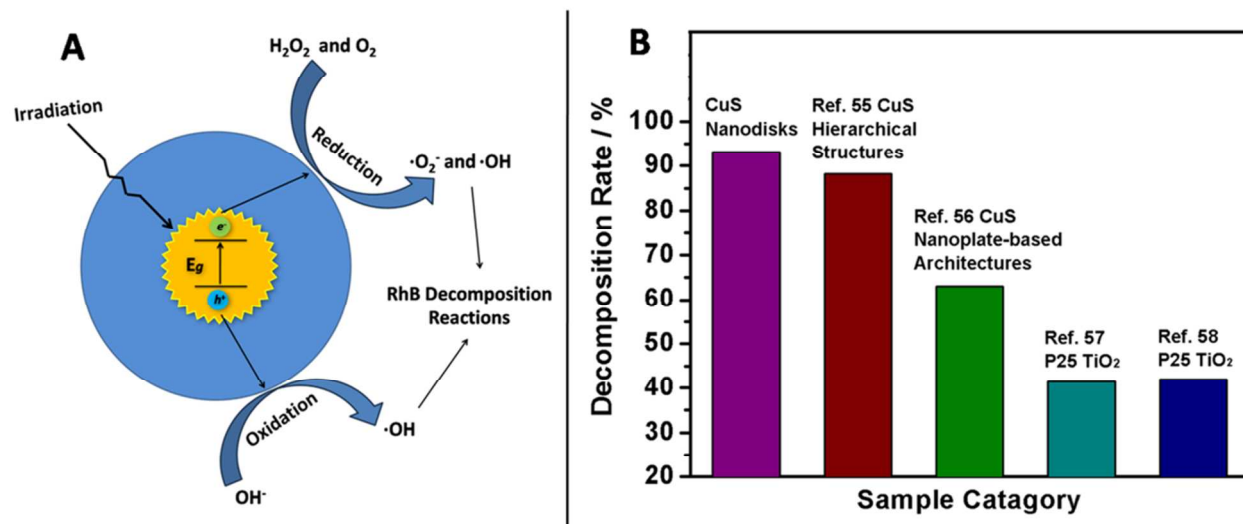
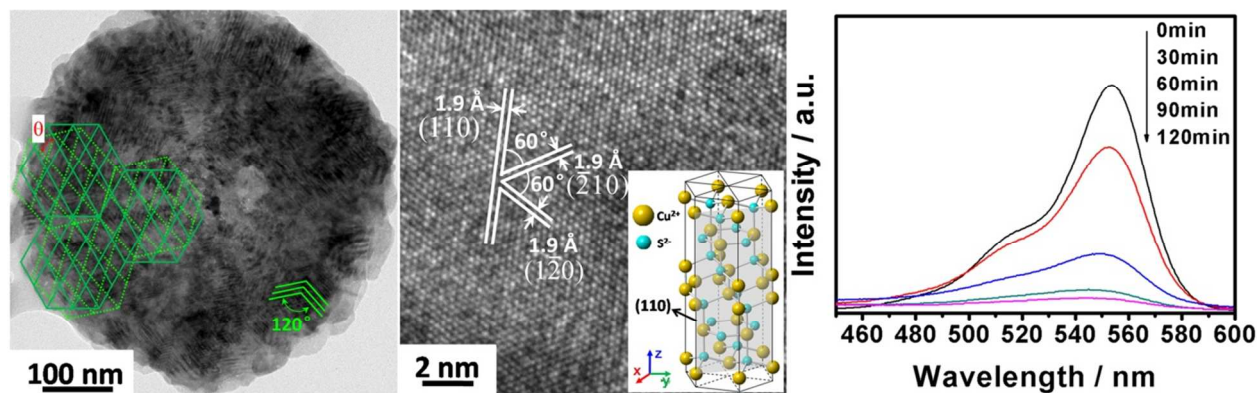


Figure 8. Schematic illustration of mechanism for the photocatalysis in CuS nanopowders under visible light irradiation (A) and comparison of photocatalytic performances of samples reported in other research (B).



Graphic Abstract